iScience

CellPress
OPEN ACCESS

Article

Low concentration electrolyte with non-solvating cosolvent enabling high-voltage lithium metal batteries

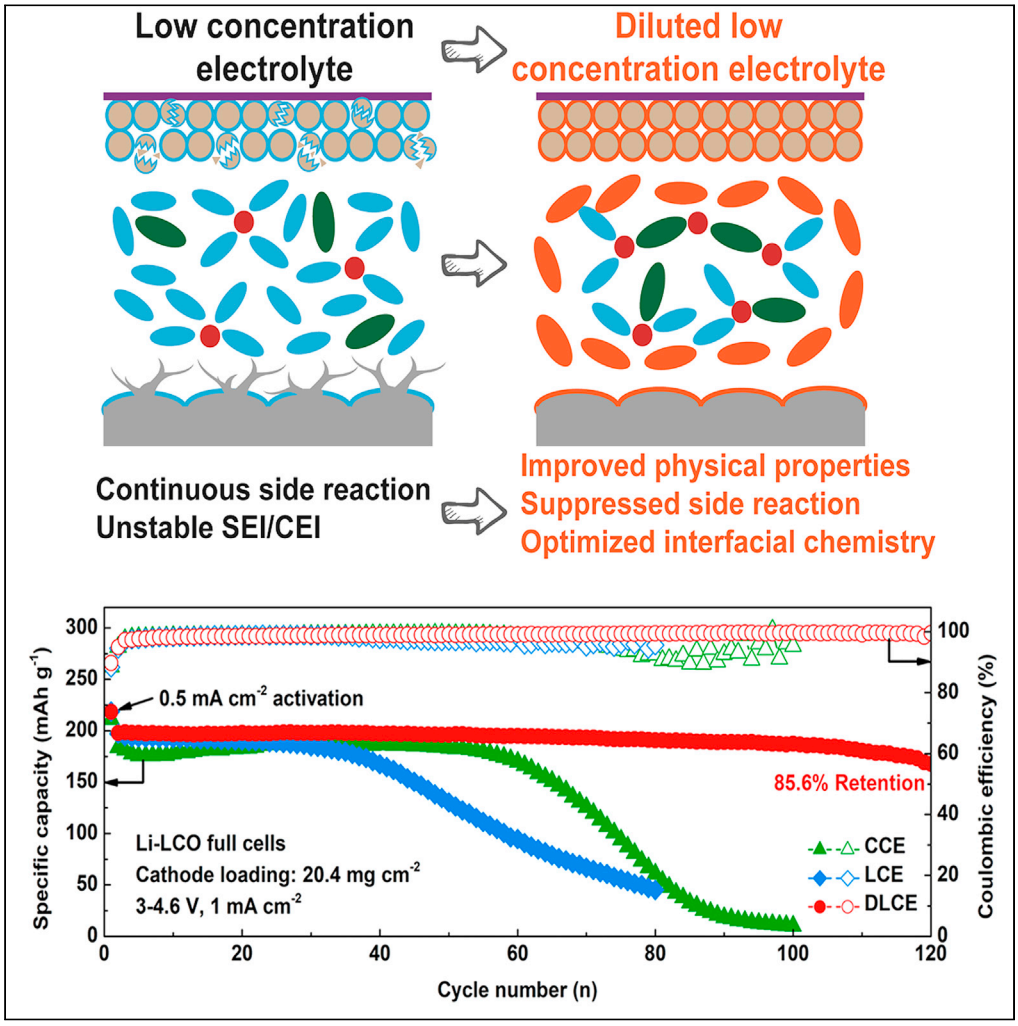

Zhipeng Jiang, Ziqi Zeng, Han Zhang, ..., Chuang Yu, Shijie Cheng, Jia Xie

xiejia@hust.edu.cn

Highlights

A low concentration electrolyte is designed for high-voltage lithium metal batteries

Low concentration electrolyte has advantages in terms of cost and viscosity

The addition of diluent can regulate the solvation structure and interface properties

A Li-$LiCoO_2$ pouch cell achieves an energy density of more than 400 Wh kg^{-1}

Jiang et al., iScience 25, 103490
January 21, 2022
https://doi.org/10.1016/j.isci.2021.103490

iScience

CellPress
OPEN ACCESS

Article

Low concentration electrolyte with non-solvating cosolvent enabling high-voltage lithium metal batteries

Zhipeng Jiang,[1,2,4] Ziqi Zeng,[1,4] Han Zhang,[1,2] Li Yang,[3] Wei Hu,[1] Xinmiao Liang,[3] Jiwen Feng,[3] Chuang Yu,[1] Shijie Cheng,[1] and Jia Xie[1,5,*]

SUMMARY

Developing low cost, yet high-voltage electrolyte is significant to improve the energy density and practicability of lithium metal batteries (LMBs). Low concentration electrolyte has significant merits in terms of cost and viscosity; however, their poor compatibility with high-voltage LMBs hinders its applications. Here, we develop a diluted low concentration electrolyte by replacing solvating cosolvent with a non-solvating cosolvent to facilitate the interaction between BF_4^- and Li^+, resulting in optimized interfacial chemistry and suppressed side reaction. Thus, the high-loading Li-$LiCoO_2$ full cells (20.4 mg cm^{-2}) deliver outstanding cycling stability and rate performance at a cutoff voltage of 4.6 V. More impressively, a Li-$LiCoO_2$ pouch cell achieves an energy density of more than 400 Wh kg^{-1} under practical conditions with thin Li (50 μm) and lean electrolyte (2.7 g Ah^{-1}). This work provides a rational approach to design a low concentration electrolyte, which can be extended to other high voltage battery systems.

INTRODUCTION

Lithium-ion batteries (LIBs) has gradually approached their ceiling of energy density afforded by intercalation chemistry, falling behind the increasing demands for advanced portable electronics and electric vehicles (Duffner et al., 2021). In this context, lithium metal batteries (LMBs) outperform other candidates in terms of energy density because metallic Li anode possesses the highest theoretical specific capacity (3860 mAh g^{-1}) and lowest redox potential (−3.04 V vs. the standard hydrogen electrode) (Wu et al., 2020b; Xu et al., 2021a; Zhong et al., 2021). Besides, further increasing the working voltage of LMBs is also critical for higher energy density. We note here that layer-structured $LiCoO_2$ (LCO) can achieve a high capacity of 220 mAh g^{-1} at an escalated upper cutoff voltage of 4.6 V (Wang et al., 2020a; Li et al., 2021). Along with its high Li^+/electron conductivity, theoretical density, and compressed electrode density, high-voltage LCO still possesses many competitive advantages in the family of cathode material (Lyu et al., 2021; Chikkannanavar et al., 2014). However, accompanied decrease in cyclability and thermal abuse tolerance renders these approaches challenging, due to the well-known problems of lithium metal anode (LMA), such as inhomogeneous Li^+ deposition kinetics and unstable solid-electrolyte interphase (SEI) (Lin et al., 2017; Xu et al., 2021b), as well as the structure collapse and detrimental cathode/electrolyte interface reactions of high-voltage LCO (Lim et al., 2019; Kalluri et al., 2017).

Developing multifunctional electrolytes is an effective way to overcome challenges of high-voltage LMBs (Zhang et al., 2020; Yamada et al., 2019). Typically, various high-efficiency additives ware added to the conventional carbonate electrolytes with a Li salt concentration of 1 M, such as fluoroethylene carbonate (FEC), $LiNO_3$, and nitro-C_{60} (Zhang et al., 2017; Jiang et al., 2019, 2020a). Besides, high oxidation tolerance solvent, such as sulfone- and nitrile-based electrolytes were used to substitute carbonate solvents (Alvarado et al., 2018;Aspern et al., 2019; Hu et al., 2020). Most strikingly, the strategy of "solvent-in-salt" was employed to broaden the electrochemical window of electrolytes, including various highly concentrated electrolytes (HCE) and diluted high concentration electrolytes (DHCE) with an increased Li salt concentration of 2–10 M (Suo et al., 2018; Chen et al., 2018; Piao et al., 2020).

Nevertheless, recent studies raise valuable reconsideration on the vital role of high salt concentration for energy storage devices. The so called "low concentration electrolyte (LCE)" has received extensive attention because of its huge advantages in cost, compared with the conventional concentration electrolyte

[1]State Key Laboratory of Advanced Electromagnetic Engineering and Technology, School of Electrical and Electronic Engineering, Huazhong University of Science and Technology, Wuhan 430074, P. R. China

[2]State Key Laboratory of Materials Processing and Die & Mould Technology, School of Materials Science and Engineering, Huazhong University of Science and Technology, Wuhan 430074, China

[3]State Key Laboratory of Magnetic Resonance and Atomic and Molecular Physics, Wuhan Institute of Physics and Mathematics, Innovation Academy for Precision Measurement Science and Technology, Chinese Academy of Sciences, Wuhan 430071, P. R. China

[4]These authors contributed equally

[5]Lead contact

*Correspondence: xiejia@hust.edu.cn

https://doi.org/10.1016/j.isci.2021.103490

(CCE) and HCE (Hu and Lu, 2020). Hu's group put forward the concept of LCE and applied it in sodium-ion batteries (SIBs) (Li et al., 2020). Wu et al. reported that the reduction of salt concentrations to 0.1 M suppressed the polysulfide shuttle effects in lithium-sulfur (Li-S) batteries (Wu et al., 2020a). Xiang and coworkers designed a dual-salt LCE to construct a robust SEI in Li-$LiFePO_4$ full cells (Zheng et al., 2020). However, the use of low concentration electrolytes for high-voltage LMBs still faces great challenges due to the continuous decomposition of free solvents and the instability of the electrolyte/electrode interface. The solvation structure of the electrolyte plays an essential role in determining these properties. Specifically, the amount of free solvents can be effectively reduced by the use of strong coordinated lithium salts (LiFSI, LiDFOB, $LiBF_4$, etc.) or the addition of non-solvating cosolvents (Ding et al., 2021; Weber et al., 2019; Louli et al., 2020), while the introduction of fluorinated reagents can form a stable LiF protective layer (Yan et al., 2020).

It is widely accepted from recent studies that the anion-dominated solvation structure is the key to obtain electrochemical stability of HCEs and DHCEs (Jiang et al., 2021). In light of this, it is possible to develop a low concentrated electrolyte with excellent electrochemically compatibility by replacing solvating cosolvent with an equal volume of non-solvating cosolvent. So, the deficient coordination between Li^+ and solvating cosolvent must facilitate the anion-cation interaction and thus promote the generation of aggregates (AGGs, an anion coordinating to two or more Li^+). Based on these insights, we design a diluted low concentration electrolyte (DLCE) that enables stable cycling of high-voltage LMBs. In detail, replacing half of the solvents in the typical dult-salt LCE (0.3 M LiDFOB +0.2 M $LiBF_4$ in DEC/FEC (7: 3 by volume)) with non-solvating fluorobenzene (FB) obtains the DLCE (0.3 M LiDFOB +0.2 M $LiBF_4$ in DEC/FEC/FB (3.5: 1.5: 5 by volume)) with significantly improved electrochemical performance. As illustrated in Figure 1A, the addition of FB cosolvent not only improves the physical properties of LCE, but also regulates the solvation structure, which contributes to the formation of LiF-rich interface. Benefiting from these optimized properties, the high-loading Li-$LiCoO_2$ (LCO, 20.4 mg cm^{-2}) cell based on DLCE displays excellent cycle stability and rate performance at the cutoff voltage as high as 4.6 V. More impressively, a Li-LCO pouch cell sustains an estimated energy density over 400 Wh kg^{-1} under practical test conditions (50 μm Li, 2.7 g Ah^{-1} electrolyte).

RESULTS AND DISCUSSION

Solvation structure of electrolyte

FB, as a cosolvent holds the advantages of low density and low cost compared with hydrofluorinated ether (HFE) (Jiang et al., 2021). To ensure that the lithium salt can be fully dissolved, the concentration of electrolyte was selected as 0.3 M LiDFOB and 0.2 M $LiBF_4$ in the DEC/FEC/FB system based on the results of the solubility test (Figure S1). Besides, the CCE (0.6 M LiDFOB +0.4 M $LiBF_4$ in DEC/FEC (7: 3 by volume)) is chosen as a control electrolyte to demonstrate the effect of FB on the physicochemical property and solvation structure. Thanks to the decreased salt concentration and the low viscosity of FB, the DLCE exhibits the lowest density of 1.11 g cm^{-3}, the lowest viscosity of 1.27 mPs·S, and outstanding wettability with contact angle of 21.5°(Figures S2 and S3). As expected, Raman spectrums indicate that FB is barely coordinated with Li^+ (Figure S4) and the Li^+-solvents interaction is significantly facilitated in the DLCE (Figure 1B), thereby reducing the content of free FEC (Yang et al., 2019). Besides, in all three electrolytes, the peaks of free BF_4^- are quite weak, and contact ion pairs (CIPs, one BF_4^- coordinating to one Li^+, 763 cm^{-1}) occupy dominant stage owing to the strong association strength of $LiBF_4$ and the poor donor ability of FEC and DEC (Figure 1C). More critically, a certain amount of CIPs convert to AGGs (aggregates) after replacing half of the solvent with FB, suggesting that interaction between Li^+ and BF_4^- becomes even stronger in the DLCE (Figure 1C) (Seo et al., 2012). These positively charged AGGs are supposed to allow more BF_4^- to enter the electric double layer at the solid-liquid interphase, thus enhancing decomposition kinetics of BF_4^- to form a LiF-rich SEI. Meanwhile, increasing the salt concentration from 0.5 M (LCE) to 1 M (CCE) has similar effects. The ^{11}B NMR spectra can further verify this conclusion. As shown in Figure 1D, the characteristic peak of BF_4^- upshifts from −2.36 to −2.41 ppm with increasing salt concentration from 0.5 M to 1 M. More critically, this peak shifts to −2.52 ppm upon more AGGs in the DLCE (Zhou et al., 2011). But, the solvated structure of LiDFOB is almost unchanged in studied electrolytes based on the results of Raman and ^{11}B NMR, which may be owing to a weaker solvation ability for LiDFOB (Figure S5). The change of coordination structures greatly determines the decomposition potential of electrolyte. The electrochemical stabilities of the DLCE at high voltages were evaluated by linear sweep voltammetry (LSV). On the high-voltage side, the LSV scans show that the electrochemical decomposition of electrolyte starts at 4.50 V in the LCE, 5.00 V in the CCE, and 5.25 V in the DLCE (Weber et al., 2019; Louli et al., 2020; Zhang et al., 2002), which should nevertheless be sufficient for most commercial high-voltage cathodes. The

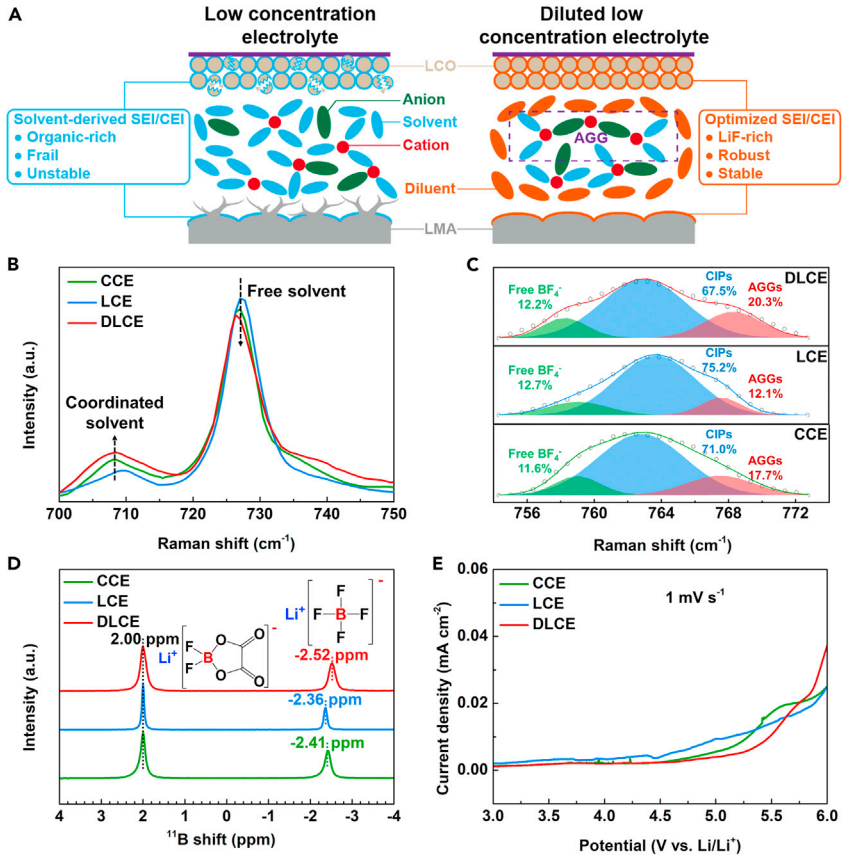

Figure 1. Solvation-structural characterization

(A–C) (A) Solvation and interfacial structures of the LCE and DLCE for Li-LCO batteries during cycling. Raman spectra of different electrolytes in the wavenumber range of (B) 700–750 cm^{-1} (FEC $_{O\text{-}C\text{-}O}$) and (C) 754–774 cm^{-1} (BF_4^-).
(D and E) (D) ^{11}B NMR spectra and (E) LSV plots of various electrolytes.

improved anodic stability of DLCE can be divided into three aspects; firstly, the content of free solvents is deceased. Secondly, the coordinated solvents may have a lower tendency to be oxidized. Thirdly, the FB may have more excellent anodic stability than FEC and DEC.

The cycling reversibility of LMA in different electrolytes was demonstrated by the Coulombic efficiency (CE) (Xiao et al., 2020). As shown in Figure 2A, under the test conditions of 1 mA cm^{-2}, 1 mAh cm^{-2}, the average CE of Li plating/stripping in the DLCE is as high as 98.3%, considerably higher than 94.2% in the LCE and 98.2% in the CCE, indicating that introducing FB improves the reversibility of Li plating/stripping. Tafel plots further demonstrate that the electrochemical reaction kinetics of Li electrode is quite fast in the DLCE, as evidenced by its highest exchange current density of 1.97 mA cm^{-2}, thus eliminating uneven Li deposition (Figure 2B) (Jiang et al., 2020b). X-ray photoelectron spectroscopy (XPS) was conducted to analyze the composition of the SEI on LMAs. It is seen from Figure 2C that the SEI formed in the DLCE and CCE have roughly similar contents of F, Li, C, and O. The generation of F is mainly attributed to the decomposition of FEC and Li salts in electrolytes. It is worth noting that the SEI formed in the DLCE and CCE all contains less organic compounds (O contained species) and more LiF compared with the LCE, as a result of diminished solvent reduction and significant salt reduction products (Figures 2C, S6, and S7). The corresponding element distribution of Li deposition detected by energy-dispersive X-ray spectroscopy (EDX) also verifies that the SEI formed in the CCE and DLCE contains more F and fewer C elements, implying that the SEI layer derived from anions can effectively inhibit further side reactions of solvent (Figure S8). The morphology of Li deposition was in-depth studied by scanning electron microscopy (SEM) to clarify the mechanism of the performance improvement (Figures 2D–2F and S9). As expected, dense and uniform Li depositions are observed in the DLCE and CCE, and the thickness of Li film is only 15.1 μm and 18.1 μm, respectively, which is very close to the theoretical thickness of Li

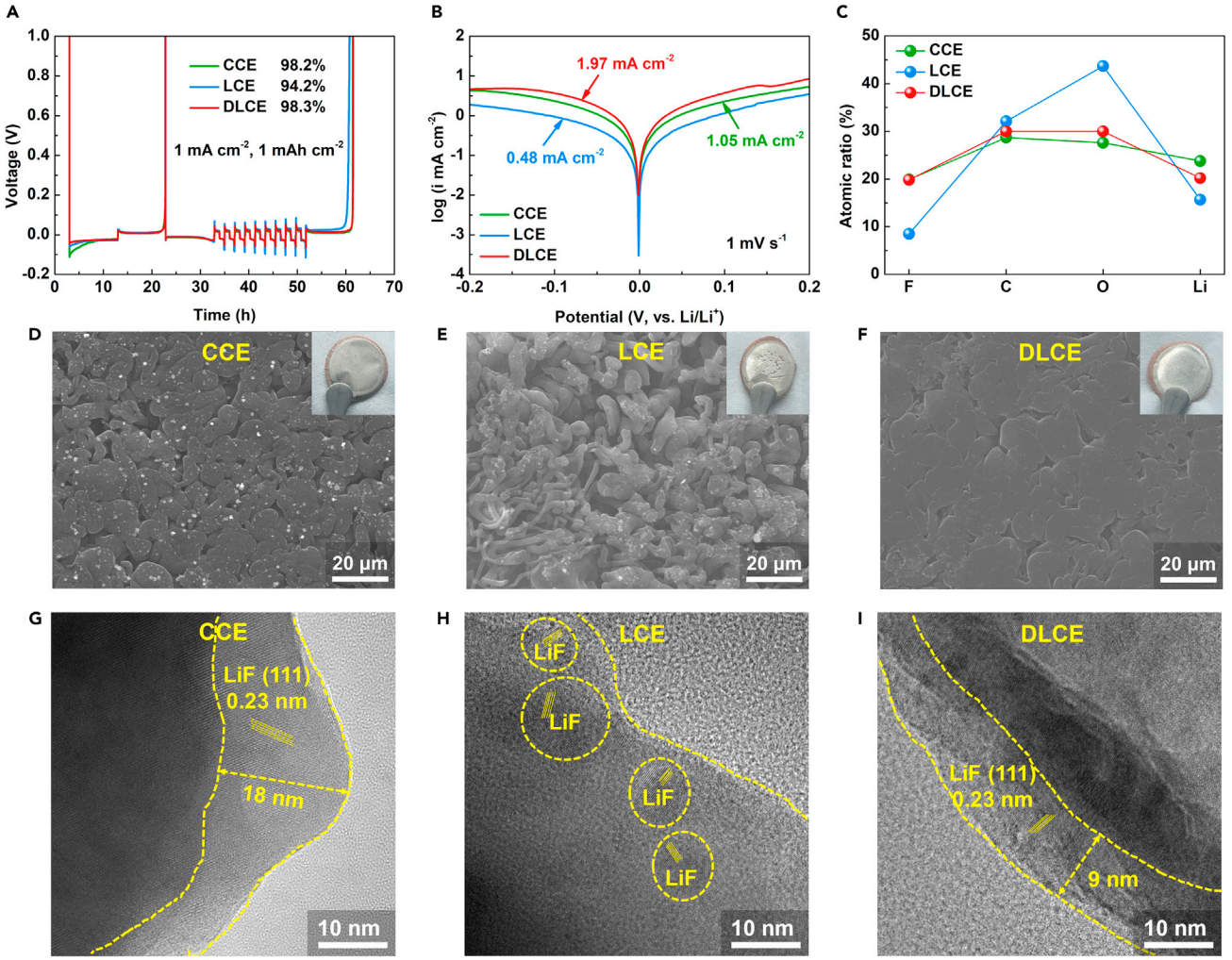

Figure 2. Li deposition performance and morphology

(A and B) (A) CE tests and (B) Tafel plots of various electrolytes.

(C–I) (C) Quantified atomic ratios of the elements in SEI from different electrolytes by XPS. SEM images of deposited Li on Cu foila in the (D) CCE, (E) LCE, and (F) DLCE (0.5 mA cm^{-2} for 3 mAh cm^{-2}). The inset is optical photographs of the deposited Li. HR-TEM images of the corresponding deposited Li in the (G) CCE, (H) LCE, and (I) DLCE.

(1 mAh cm^{-2} = 4.85 μm). In sharp contrast, large amounts of Li dendrites grow in the LCE, and the thickness of Li film is 30.1 μm. These observations are in good agreement with the variation law of the CE. Besides, the high-resolution transmission electron microscopy (HR-TEM) image of deposited Li in the LCE shows that the LiF is distributed randomly in the SEI together with organic component, while the SEI generated in the CCE and DLCE displays a thin layered-structure of 18 nm and 9 nm, respectively, which is rich in LiF (Figures 2G–2I and S10). The above results suggest that the addition of FB leads to anion recruitment into the Li^+ solvation sheath to form more AGGs, thus promoting the formation of a thin and LiF-rich SEI with fast kinetics, thereby significantly improving the performance of LMA.

Electrochemical performance of Li-LCO cells

To demonstrate the practicability of the developed electrolyte, the cycling performance of Li-LCO cells were tested at different temperatures. Firstly, as shown in Figures 3A, the Li^+ conductivity of DLCE is lower than that of the CCE/LCE in the temperature range from 40°C to −40°C. However, the cyclic voltammetry (CV) curve shows that the LCO cathode with smaller polarization in the DLCE than in the LCE, which suggests that the interfacial property rather than Li^+ conductivity determines the electrochemical reaction kinetics in our studied system (Figure 3B). At the conditions of 1 C/25°C, the Li-LCO cell using DLCE can

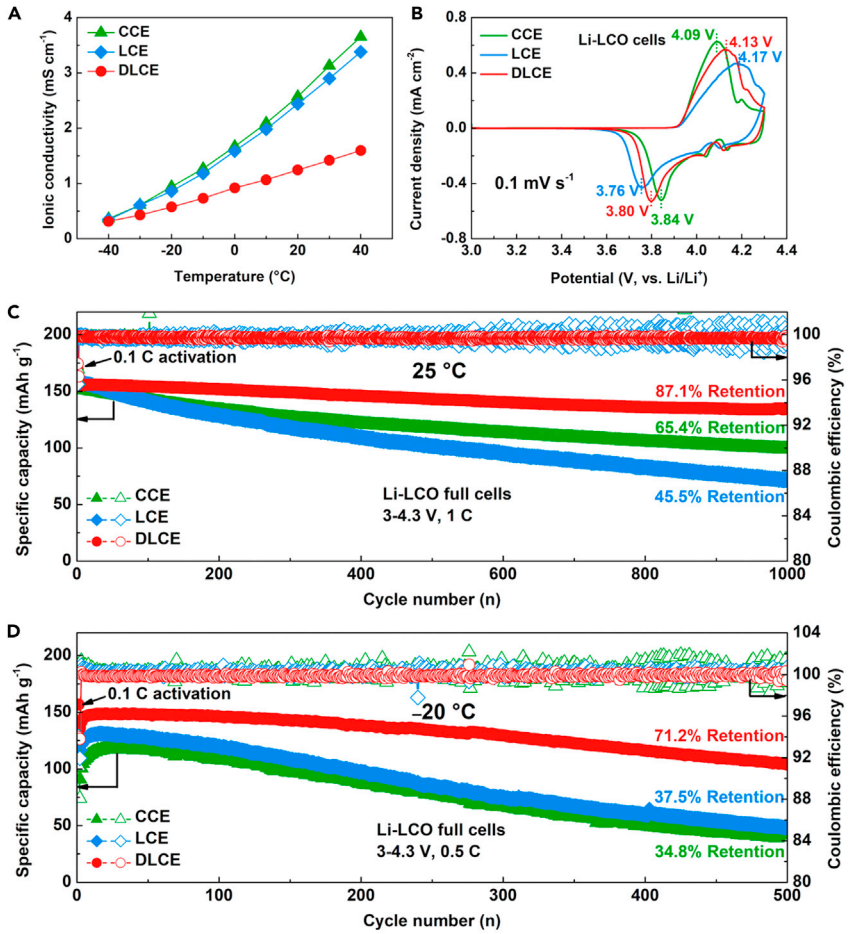

Figure 3. Li-LCO cells cycling at different temperature

(A) Li^+ conductivity of various electrolytes under different temperatures.

(B–D) (B) CV curves of the initial cycles for Li-LCO cell under different electrolytes (3–4.3 V, 0.1 mV s^{-1}). Long-term cycling performance of Li-LCO cells in different electrolytes (C) at 1 C/25°C and (D) 0.5 C/−20°C (1 C = 170 mA g^{-1}).

maintain 87.1% of the initial capacity after 1000 cycles, while the cell in the CCE and LCE only has capacity retention of 65.4% and 45.5%, respectively (Figures 3C and S11). The corresponding electrochemical impedance spectroscopy (EIS) plots imply that the interphase resistances (R_{CEI}) and charge-transfer resistances (R_{CT}) in DLCE are significantly lower than that in CCE and LCE during cycling, which further demonstrates that the addition of FB cosolvent improves the interphase stability of LCO (Figure S12). Even at the low temperature of −20°C (Figures 3D and S13), the Li-LCO cell using DLCE still holds outstanding cycling stability with a capacity retention of 71.2% after 500 cycles and an initial specific capacity as high as 158 mAh g^{-1}. In sharp contrast, the cell using LCE only presents the capacity retention of 37.5% and an initial specific capacity of 136 mAh g^{-1}. More importantly, the Li-LCO cell in the CCE exhibits the poorest electrochemical performance with the capacity retention of 34.8% and the initial specific capacity of 118 mAh g^{-1} at low temperature, indicating that the physical properties of the electrolyte can significantly affect the low-temperature performance of LMBs.

Increasing cathode loading and cutoff voltage are two effective ways to enhance the energy density of LMBs. Therefore, Li-LCO cells using different electrolytes were assembled using commercial LCO cathode (loading: 20.4 mg cm^{-2}) with a cutoff voltage of 4.6 V. Benefiting from the modified solvation structure and interfacial chemistry, the Li-LCO cells show excellent rate performance in both of the DLCE and CCE with a specific capacity of 65 mAh g^{-1} even at the high current density of 5 mA cm^{-2} (Figures 4A and S14). In comparison, the Li-LCO using LCE only delivers a specific capacity of 30 mAh g^{-1}. Besides, the addition of non-solvating cosolvent effectively suppresses the occurrence of side reactions at the interface, thereby improving the long-term cycling

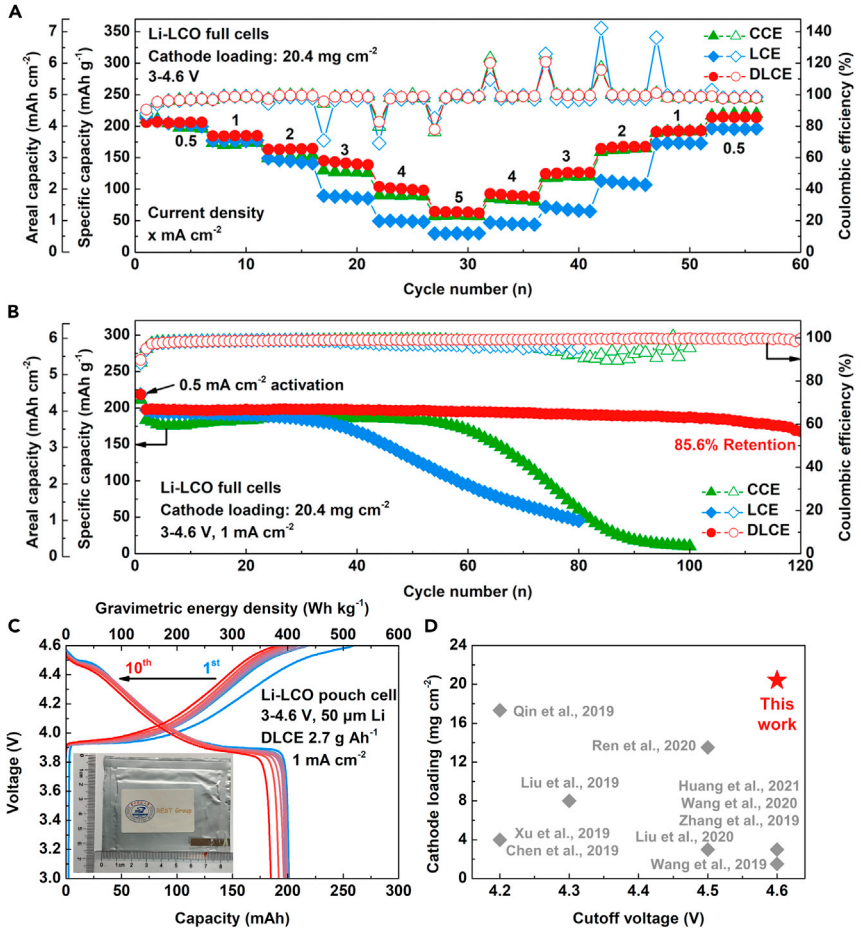

Figure 4. High-voltage Li-LCO full cells at practical conditions

(A and B) (A) Rate performance and (B) long-term cycling performance of high-loading Li-LCO cells under different electrolytes (Cathode loading: 20.4 mg cm^{-2}, 3–4.6 V).

(C) The charge-discharge curves of Li-LCO pouch cell using DLCE under practical conditions (Cathode loading: 20.4 mg cm^{-2}, 3–4.6 V, 50 μm Li, 2.7 g Ah^{-1} electrolyte).

(D) The performance comparison of Li-LCO cells.

stability of LMBs. Therefore, the Li-LCO cell using DLCE can operate steady over 120 cycles with the capacity retention of 85.6% at the current density of 1 mA cm^{-2}, while the Li-LCO cells using CCE and LCE display rapid capacity fading after 60 cycles and 30 cycles, respectively (Figures 4B and S15). In addition, fluorine nuclear magnetic resonance (^{19}F NMR) spectra were used to evaluate the consumption of LiDFOB after cycled in high-loading Li-LCO cells with different electrolytes (Figure S16). After 100 cycles, LiDFOB in the LCE is almost exhausted, but it can still be detected in DLCE and CCE, showing the unique solvated structure and interface chemistry of DLCE can effectively reduce the decomposition of LiDFOB and the subsequent gas production issues. Finally, a Li-LCO pouch cell was assembled under practical conditions, including high-loading cathode (20.4 mg cm^{-2}), high cutoff voltage (4.6 V), thin Li foil (50 μm), and lean electrolyte (2.7 g Ah^{-1}). Based on these parameters, the energy density of Li-LCO is calculated to be 400 Wh kg^{-1} (Figure 4C and Table S1). The Li-LCO cells using DLCE simultaneously satisfy the conditions of high cathode loading and high cutoff voltage, and show superior performance to most previous studies (Figure 4D and Table S2) (Qin et al., 2019; Xu et al., 2019; Chen et al., 2019; Liu et al., 2019, 2020; Ren et al., 2020; Huang et al., 2021; Wang et al., 2019, 2020b; Zhang et al., 2019).

Characterization of LCO after cycled

Finally, we characterized the LCO cathode and their surface layers after cycled to reveal the origin of the excellent electrochemical performance of high-voltage Li-LCO cells in the DLCE. As shown in Figures

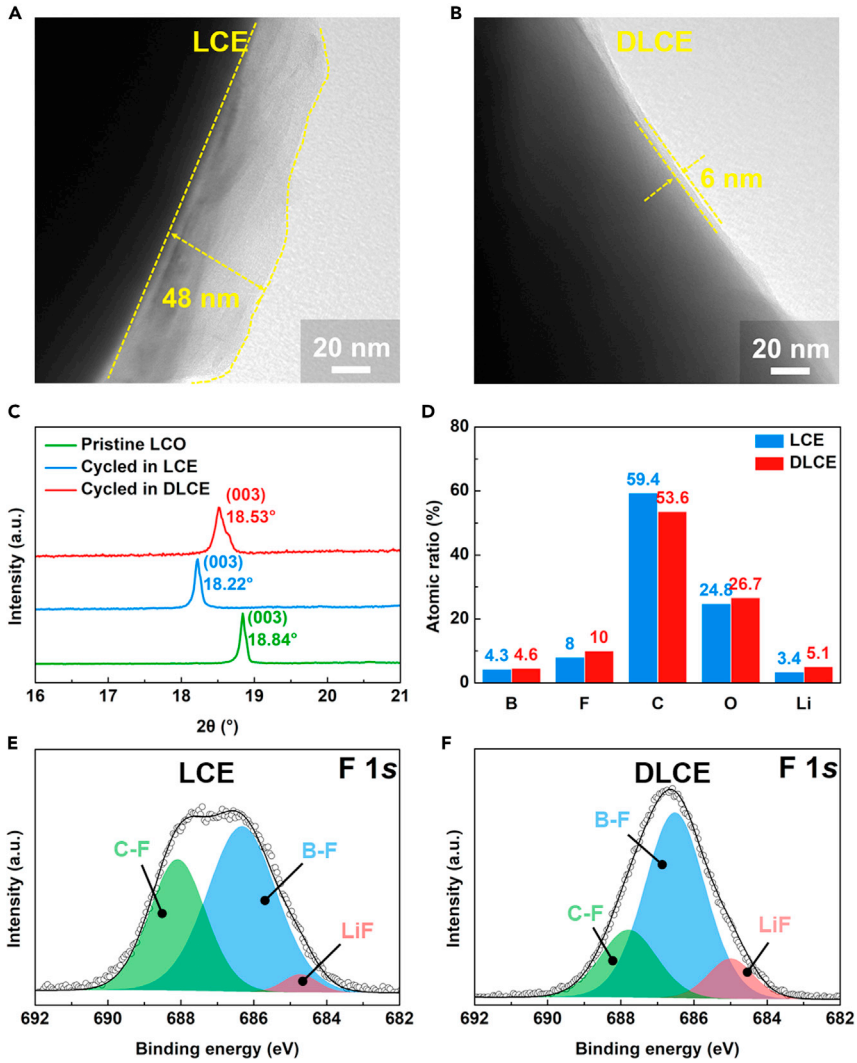

Figure 5. Characterization of cycled LCO cathode

(A–F) TEM images of cycled LCO in (A) LCE and (B) DLCE. (C) XRD patterns of different LCO. (D) Quantified atomic ratios of the elements in CEI from different electrolytes by XPS. F 1s spectra of the cycled LCO in (E) LCE and (F) DLCE (Cycling conditions: 20.4 mg cm^{-2} cathode, 3–4.6 V, 80 cycles).

5A, 5B, and S17, a thin (6 nm) and homogeneous CEI is observed on the surface of LCO after cycled in the DLCE, while the thickness of CEI formed in the LCE is 48 nm, as a result of the continuous oxidation decomposition of free solvents (Ren et al., 2020). This structural difference in CEI will significantly affect the cycling stability of LCO under high voltage. In detail, a relatively small (003) peak shift is observed in LCO cycled in DLCE at a high voltage of 4.6 V, in contrast with the dramatic (003) peak shift in LCO cycled in LCE, demonstrating suppressed O3 to H1–3 phase transition in the DLCE (Figures 5C and S18) (Zhang et al., 2019; Yoon et al., 2020). Besides, the CEI formed in the DLCE also contains more F and fewer C elements (Figure 5D). The increase in F content stems from the decomposition of FB and salt to produce additional LiF, while the decrease in C content further proves that the decomposition of the solvent in the DLCE is inhibited (Figures 5E, 5F, and S19) (Zhou et al., 2011).

Conclusions

In conclusion, we have demonstrated that replacing solvating cosolvent in LCE with an equal volume of non-solvating cosolvent is highly effective to enhance the interaction between BF_4^- and Li^+, thus inducing a BF_4^--derived LiF-rich SEI in the diluted low concentration electrolyte. Besides, the side reaction of the electrolyte can be significantly inhibited and LCO is well protected. Thanks to these modified solvation

structures and improved interfacial properties, a high loading cell using DLCE presents outstanding cycling stability even under a cutoff voltage of 4.6 V. Besides, the Li-LCO pouch cell exhibits a high specific energy of more than 400 Wh kg^{-1}. This work not only provides a feasible way for the practical application of low concentration electrolytes but also develops a new view for the design of advanced electrolytes.

Limitations of the study

In this work, we developed a diluted low concentration electrolyte for high-voltage lithium metal batteries. Future studies can explore the feasibility of this new insight of electrolytes in other battery systems, such as lithium-ion batteries, sodium-ion batteries, and aqueous batteries.

STAR★METHODS

Detailed methods are provided in the online version of this paper and include the following:

- KEY RESOURCES TABLE
- RESOURCE AVAILABILITY
  - Lead contact
  - Materials availability

SUPPLEMENTAL INFORMATION

Supplemental information can be found online at https://doi.org/10.1016/j.isci.2021.103490.

ACKNOWLEDGMENTS

This work was supported by the National Natural Science Foundation of China (Nos. 21975087, U1966214, 51902116). We gratefully acknowledge the Analytical and Testing Center of HUST for allowing us to use its facilities.

AUTHOR CONTRIBUTIONS

X. J., Z. J., and Z. Z. proposed the research. Z. J. and Z. Z. designed the experiments. H. Z. and W. H. performed the electrochemical measurements, conducted the SEM and EDX observations, and XPS measurements with help from C. Y and S. C. L.Y., X. L., and J. F. conducted the NMR measurements. Z. Z. helped with XRD analysis. W. H. prepared the LCO electrodes. All authors discussed the results. Z. J. and Z. Z. prepared the manuscript with revisions by C. Y., S. C., and X. J. All authors gave approval to the final version of the manuscript.

DECLARATION OF INTERESTS

The authors declare no competing financial interests.

Received: August 2, 2021
Revised: November 2, 2021
Accepted: November 19, 2021
Published: January 21, 2022

REFERENCES

Alvarado, J., Schroeder, M.A., Zhang, M., Borodin, O., Gobrogge, E., Olguin, M., Ding, M., Gobet, M., Greenbaum, S., Meng, Y., and Xu, K. (2018). A carbonate-free, sulfone-based electrolyte for high-voltage Li-ion batteries. Mater. Today *21*, 341–353. https://doi.org/10.1016/j.mattod.2018.02.005.

Aspern, N., Roschenthaler, G., Winter, M., and Cekic, I. (2019). Fluorine and lithium: ideal partners for high-performance rechargeable battery electrolytes. Angew. Chem. Int. Ed. *58*, 15978. https://doi.org/10.1002/anie.201901381.

Chen, S., Zheng, J., Mei, D., Han, K., Engelhard, M., Zhao, W., Xu, W., Liu, J., and Zhang, J. (2018). High-voltage lithium-metal batteries enabled by localized high-concentration electrolytes. Adv. Mater. *30*, 1706102. https://doi.org/10.1002/adma.201706102.

Chen, K., Pathak, R., Gurung, A., Adhamash, E., Bahrami, B., He, Q., Qiao, H., Smirnova, A., Wu, J., Qiao, Q., and Zhou, Y. (2019). Flower-shaped lithium nitride as a protective layer via facile plasma activation for stable lithium metal anode. Energy Storage Mater. *18*, 389–396. https://doi.org/10.1016/j.ensm.2019.02.006.

Chikkannanavar, S.B., Bernardi, D.M., and Lu, L. (2014). A review of blended cathode materials for use in Li-ion batteries. J. Power Sources *248*, 91–100. https://doi.org/10.1016/j.jpowsour.2013.09.052.

Ding, J.-F., Xu, R., Yao, N., Chen, X., Xiao, Y., Yao, Y.-X., Yan, C., Xie, J., and Huang, J.-Q. (2021). Non-solvating and low-dielectricity cosolvent for anion-derived solid electrolyte interphases in lithium metal batteries. Angew. Chem. Int. Ed. *60*, 11442–11447. https://doi.org/10.1002/anie.202101627.

Duffner, F., Kronemeyer, N., Tübke, J., Leker, J., Winter, M., and Schmuch, R. (2021). Post-lithium-ion battery cell production and its compatibility with lithium-ion cell production infrastructure.

Nat. Energy *6*, 123–134. https://doi.org/10.1038/s41560-020-00748-8.

Hu, Y., and Lu, Y. (2020). The mystery of electrolyte concentration: from superhigh to ultralow. ACS Energy Lett. *5*, 3633–3636. https://doi.org/10.1021/acsenergylett.0c02234.

Hu, Z., Xian, F., Guo, Z., Lu, C., Du, X., Cheng, X., Zhang, S., Dong, S., Cui, G., and Chen, L. (2020). Nonflammable nitrile deep eutectic electrolyte enables high-voltage lithium metal batteries. Chem. Mater. *32*, 3405–3413. https://doi.org/10.1021/acs.chemmater.9b05003.

Huang, Y., Zhu, Y., Fu, H., Ou, M., Hu, C., Yu, S., Hu, Z., Chen, C., Jiang, G., Gu, H., et al. (2021). Mg-pillared $LiCoO_2$: towards stable cycling at 4.6 V. Angew. Chem. Int. Ed. *60*, 4682. https://doi.org/10.1002/ange.202014226.

Jiang, Z., Zeng, Z., Yang, C., Han, Z., Hu, W., Lu, J., and Xie, J. (2019). Nitrofullerene, a C_{60}-based bifunctional additive with smoothing and protecting effects for stable lithium metal anode. Nano Lett. *19*, 8780–8786. https://doi.org/10.1021/acs.nanolett.9b03562.

Jiang, Z., Jin, L., Zeng, Z., and Xie, J. (2020a). Facile preparation of a stable 3D host for lithium metal anodes. Chem. Commun. *56*, 9898–9900. https://doi.org/10.1039/D0CC03864D.

Jiang, Z., Guo, H., Zeng, Z., Han, Z., Hu, W., Wen, R., and Xie, J. (2020b). Reconfiguring organosulfur cathode by over-lithiation to enable ultrathick lithium metal anode toward practical lithium−sulfur batteries. ACS Nano *14*, 13784–13793. https://doi.org/10.1021/acsnano.0c06133.

Jiang, Z., Zeng, Z., Liang, X., Yang, L., Hu, W., Zhang, C., Han, Z., Feng, J., and Xie, J. (2021). Fluorobenzene, a low-density, economical, and bifunctional hydrocarbon cosolvent for practical lithium metal batteries. Adv. Funct. Mater. *31*, 2005991. https://doi.org/10.1002/adfm.202005991.

Kalluri, S., Yoon, M., Jo, M., Park, S., Myeong, S., Kim, J., Dou, S., Guo, Z., and Cho, J. (2017). Surface engineering strategies of layered $licoo_2$ cathode material to realize high-energy and high-voltage li-ion cells. Adv. Energy Mater. *7*, 1601507. https://doi.org/10.1002/aenm.201601507.

Li, Y., Yang, Y., Lu, Y., Zhou, Q., Qi, X., Meng, Q., Rong, X., Chen, L., and Hu, Y. (2020). Ultralow-concentration electrolyte for Na-ion batteries. ACS Energy Lett. *5*, 1156–1158. https://doi.org/10.1021/acsenergylett.0c00337.

Li, J., Lin, C., Weng, M., Qiu, Y., Chen, P., Yang, K., Huang, W., Hong, Y., Li, J., Zhang, M., et al. (2021). Structural origin of the high-voltage instability of lithium cobalt oxide. Nat. Nanotechnol. *16*, 599. https://doi.org/10.1038/s41565-021-00855-x.

Lim, J., Choi, A., Kim, H., Doo, S., Park, Y., and Lee, K. (2019). In situ electrochemical surface modification for high-voltage LiCoO2 in lithium ion batteries. J. Power Sources *426*, 162–168. https://doi.org/10.1016/j.jpowsour.2019.04.011.

Lin, D., Liu, Y., and Cui, Y. (2017). Reviving the lithium metal anode for high-energy batteries. Nat. Nanotechnol. *12*, 194–206. https://doi.org/10.1038/nnano.2017.16.

Liu, Y., Xiong, S., Wang, J., Jiao, X., Li, S., Zhang, C., Song, Z., and Song, J. (2019). Dendrite-free lithium metal anode enabled by separator engineering via uniform loading of lithiophilic nucleation sites. Energy Storage Mater. *19*, 24–30. https://doi.org/10.1016/j.ensm.2019.02.006.

Liu, X., Liu, J., Qian, T., Chen, H., and Yan, C. (2020). Novel organophosphate-derived dual-layered interface enabling air-stable and dendrite-free lithium metal anode. Adv. Mater. *32*, 1902724. https://doi.org/10.1002/adma.201902724.

Louli, A., Eldesoky, A., Weber, R., Genovese, M., Coon, M., deGooyer, J., Deng, Z., White, R.T., Lee, J., Rodgers, T., et al. (2020). Diagnosing and correcting anode-free cell failure via electrolyte and morphological analysis. Nat. Energy *5*, 693. https://doi.org/10.1038/s41560-020-0668-8.

Lyu, Y., Wu, X., Wang, K., Feng, Z., Cheng, T., Liu, Y., Wang, M., Chen, R., Xu, L., Zhou, J., et al. (2021). An overview on the advances of $licoo_2$ cathodes for lithium-ion batteries. Adv. Energy Mater. *11*, 2000982. https://doi.org/10.1002/aenm.202000982.

Piao, N., Ji, X., Xu, H., Fan, X., Chen, L., Liu, S., Garaga, M., Greenbaum, S., Wang, L., Wang, C., and He, X. (2020). Countersolvent electrolytes for lithium-metal batteries. Adv. Energy Mater. *10*, 1903568. https://doi.org/10.1002/aenm.201903568.

Qin, Q., Deng, N., Wang, L., Zhang, L., Jia, Y., Dai, Z., Liu, Y., Kang, W., and Cheng, B. (2019). Novel flexible Mn-based carbon nanofiber films as interlayers for stable lithium-metal battery. Chem. Eng. J. *360*, 900–911. https://doi.org/10.1016/j.cej.2018.12.037.

Ren, X., Zhang, X., Shadike, Z., Zou, L., Jia, H., Cao, X., Engelhard, M., Matthews, B., Wang, C., Arey, B., et al. (2020). Designing advanced in situ electrode/electrolyte interphases for wide temperature operation of 4.5 V Li||$LiCoO_2$ batteries. Adv. Mater. *32*, 2004898. https://doi.org/10.1002/adma.202004898.

Seo, D., Borodin, O., Han, S., Boyle, P., and Henderson, W. (2012). Electrolyte solvation and ionic association ii. acetonitrile-lithium salt mixtures: highly dissociated salts. J. Electrochem. Soc. *159*, A1489–A1500. https://doi.org/10.1149/2.035209je.

Suo, L., Xue, W., Gobet, M., Greenbaum, S., Wang, C., Chen, Y., Yang, W., Li, Y., and Li, J. (2018). Fluorine-donating electrolytes enable highly reversible 5-V-class Li metal batteries. Proc. Natl. Acad. Sci. U S A *115*, 1156–1161. https://doi.org/10.1073/pnas.1712895115.

Wang, L., Ma, J., Wang, C., Yu, X., Liu, R., Jiang, F., Sun, X., Du, A., Zhou, X., and Cui, G. (2019). A novel bifunctional self-stabilized strategy enabling 4.6 V $LiCoO_2$ with excellent long-term cyclability and high-rate capability. Adv. Sci. *6*, 1900355. https://doi.org/10.1002/advs.201900355.

Wang, K., Wan, J., Xiang, Y., Zhu, J., Leng, Q., Wang, M., Xu, L., and Yang, Y. (2020a). Recent advances and historical developments of high voltage lithium cobalt oxide materials for rechargeable Li-ion batteries. J. Power Sources *460*, 228062. https://doi.org/10.1016/j.jpowsour.2020.228062.

Wang, Y., Zhang, Q., Xue, Z., Yang, L., Wang, J., Meng, F., Li, Q., Pan, H., Zhang, J., Jiang, Z., et al. (2020b). An in situ formed surface coating layer enabling $LiCoO_2$ with stable 4.6 V high-voltage cycle performances. Adv. Energy Mater. *10*, 2001413. https://doi.org/10.1002/aenm.202001413.

Weber, R., Genovese, M., Louli, A., Hames, S., Martin, C., Hill, I.G., and Dahn, J. (2019). Long cycle life and dendrite-free lithium morphology in anode-free lithium pouch cells enabled by a dual-salt liquid electrolyte. Nat. Energy *4*, 683. https://doi.org/10.1038/s41560-019-0428-9.

Wu, F., Chu, F., Ferrero, G., Sevilla, M., Fuertes, A., Borodin, O., Yu, Y., and Yushin, G. (2020a). Boosting high-performance in lithium-sulfur batteries via dilute electrolyte. Nano Lett. *20*, 5391. https://doi.org/10.1021/acs.nanolett.0c01778.

Wu, T., Qi, J., Xu, M., Zhou, D., and Xiao, Z. (2020b). Selective S/Li_2S conversion via in-built crystal facet self-mediation: toward high volumetric energy density lithium-sulfur batteries. ACS Nano *14*, 15011–15022. https://doi.org/10.1021/acsnano.0c04933.

Xiao, J., Li, Q., Bi, Y., Cai, M., Dunn, B., Glossmann, T., Liu, J., Osaka, T., Sugiura, R., Wu, B., et al. (2020). Understanding and applying coulombic efficiency in lithium metal batteries. Nat. Energy *5*, 561. https://doi.org/10.1038/s41560-020-0648-z.

Xu, Y., Li, T., Wang, L., and Kang, Y. (2019). Interlayered dendrite-free lithium plating for high-performance lithium-metal batteries. Adv. Mater. *31*, 1901662. https://doi.org/10.1002/adma.201901662.

Xu, M., Liang, L., Qi, J., Wu, T., Zhou, D., and Xiao, Z. (2021a). IntralayeredOstwald Ripening-induced self-catalyzed growth of CNTs on MXene for robust lithium-sulfur batteries. Small *17*, 2007446. https://doi.org/10.1002/smll.202007446.

Xu, R., Shen, X., Ma, X.-X., Yan, C., Zhang, X.-Q., Chen, X., Ding, J.-F., and Huang, J.-Q. (2021b). Identifying the critical anion-cation coordination to regulate the electric double layer for an efficient lithium-metal anode interface. Angew. Chem. Int. Ed. *60*, 4215–4220. https://doi.org/10.1002/ange.202013271.

Yamada, Y., Wang, J., Ko, S., Watanabe, E., and Yamada, A. (2019). Advances and issues in developing salt-concentrated battery electrolytes. Nat. Energy *4*, 269. https://doi.org/10.1038/s41560-019-0336-z.

Yan, C., Yuan, H., Park, H.S., and Huang, J.-Q. (2020). Perspective on the critical role of interface for advanced batteries. J. Energy Chem. *47*, 217–220. https://doi.org/10.1016/j.jechem.2019.09.034.

Yang, G., Sacci, R., Ivanov, I., Ruther, R., Hays, K., Zhang, Y., Cao, P., Veith, G., Dudney, N., Saito, T., et al. (2019). Probing electrolyte solvents at solid/liquid interface using gap-mode surface-enhanced Raman spectroscopy. J. Electrochem.

Soc. *166*, A178–A187. https://doi.org/10.1149/2.0391902jes.

Yoon, M., Dong, Y., Yoo, Y., Myeong, S., Hwang, J., Kim, J., Choi, S., Sung, J., Kang, S., Li, J., and Cho, J. (2020). Unveiling nickel chemistry in stabilizing high-voltage cobalt-rich cathodes for lithium-ion batteries. Adv. Funct. Mater. *30*, 1907903. https://doi.org/10.1002/adfm.201907903.

Zhang, S., Xu, K., and Jow, T. (2002). Study of $LiBF_4$ as an electrolyte salt for a Li-ion battery. J. Electrochem. Soc. *149*, A586–A590. https://doi.org/10.1149/1.1466857.

Zhang, X., Cheng, X., Chen, X., Yan, C., and Zhang, Q. (2017). Fluoroethylene carbonate additives to render uniform li deposits in lithium metal batteries. Adv. Funct. Mater. *27*, 1605989. https://doi.org/10.1002/adfm.201605989.

Zhang, J., Li, Q., Ouyang, C., Yu, X., Ge, M., Huang, X., Hu, E., Ma, C., Li, S., Xiao, R., et al. (2019). Trace doping of multiple elements enables stable battery cycling of $LiCoO_2$ at 4.6 V. Nat. Energy *4*, 594–603. https://doi.org/10.1038/s41560-019-0409-z.

Zhang, J., Xu, W., Xiao, J., Cao, X., and Liu, J. (2020). Lithium metal anodes with nonaqueous electrolytes. Chem. Rev. *120*, 13312–13348. https://doi.org/10.1021/acs.chemrev.0c00275.

Zheng, H., Xiang, H., Jiang, F., Liu, Y., Sun, Y., Liang, X., Feng, Y., and Yu, Y. (2020). Lithium difluorophosphate-based dual-salt low concentration electrolytes for lithium metal batteries. Adv. Energy Mater. *10*, 2001440. https://doi.org/10.1002/aenm.202001440.

Zhong, M., Guan, J., Sun, J., Shu, X., Ding, H., Chen, L., Zhou, N., and Xiao, Z. (2021). A cost- and energy density-competitive lithium-sulfur battery. Energy Storage Mater. *41*, 588–598. https://doi.org/10.1016/j.ensm.2021.06.037.

Zhou, L., Li, W., Xu, M., and Lucht, B. (2011). Investigation of the disproportionation reactions and equilibrium of lithium difluoro (oxalato) borate (LIDFOB). Electrochem. Solid State Lett. *14*, A161–A164. https://doi.org/10.1149/2.016111esl.

STAR★METHODS

KEY RESOURCES TABLE

REAGENT or RESOURCE	SOURCE	IDENTIFIER
Other		
Li foil	China Energy Lithium Co., Ltd.	CAS#7439-93-2
Fluorobenzene	Aladdin	CAS#462-06-6
$LiCoO_2$ power	Shenzhen Kejing Star Technology Co., Ltd.	CAS# 12190-79-3
Lithium difluoro(oxalato)borate	Dodo Chem Co., Ltd.	CAS#409071-16-5
lithium tetrafluoroborate	Dodo Chem Co., Ltd.	CAS#14283-07-9
fluoroethylene carbonate	Dodo Chem Co., Ltd.	CAS#114435-02-8
diethyl carbonate	Dodo Chem Co., Ltd.	CAS#105-58-8
Commercial $LiCoO_2$ electrode	Zhuhai COSMX power battery Co., Ltd.	http://www.cosmx.com/html/about/about/

RESOURCE AVAILABILITY

Lead contact

Further information and requests for resources should be directed to and will be fulfilled by the lead contact, Jia Xie (xiejia@hust.edu.cn).

Materials availability

This study did not generate new unique reagents.

Data and code availability

Data reported in this paper will be shared by the lead contact upon request.

This paper does not report original code.

Any additional information required to reanalyze the data reported in this paper is available from the lead contact upon request.